Shot-gather angle-domain noise filtering in RTM

Mandy Wong, Biondo Biondi, and Shuki Ronen

ABSTRACT

Unwanted noise in reverse-time migration image are filtered by discriminating in the prestack subsurface angle domain. For each shot image gather, we use a specific set of angles to perform the filtering. This angle range restriction can vary with shots, depth, and midpoint location. We find that noise filtering method can help alleviate migration artifacts or crosstalk noise in the image. A field example shows that prestack angle-domain noise filtering is very useful in least-squares reverse-time migration.

INTRODUCTION

Unwanted noise sometimes appears in the migrated images. For example, when internal multiples are not properly removed, migrating the remaining multiple energy with an operator that only accounts for the kinematics of the primary would result in crosstalk noise. In ocean-bottom datasets, imperfect PZ summation or up-down decomposition can also result in artifacts in the migrated image. Another source of noise comes from our attempt to invert elastic data with acoustic waves theory. For instance, converted waves are in the data but they are not accounted for in the acoustic modeling and migration operator. Ideally, we want all unaccounted events to be removed in the field data before migration. In field dataset, it can be difficult to completely remove all the unaccounted events. For example, surface-related multiple elimination (SRME) (Riley and Claerbout, 1976; Tsai, 1985; Verschuur et al., 1992) in theory can attenuate all multiples with a bounce at the water surface. However, it requires an overlap of source and receiver locations that is not realistic for many practical acquisition geometries. Well-known demultiple tools such as Radon demultiple in the data space are limited to cases where the geology is simple (Yilmaz, 1991). When the geology is complex, multiples are not easily separated from primaries. In PZ summation, it can be challenging to separate out up- and down-going signal if strong V_z noise is present in the vertical geophone recording.

While there is a lot of literature on removing unwanted energy in the data space, very few people has worked on removing noise in the image space. Alvarez et al. (2007) worked on attenuation of specular water-bottom multiples and diffracted 2D multiples. Residual moveout equations in ADCIG are used to design apex-shifted Radon transform to separate between primaries and multiples in the image space. However, the residual moveout equation used are only optimized to attenuate water-bottom related multiples. Valenciano (2008) filter out salt-related internal multiples

in the $k_x - k_{hx}$ wavenumber space. He observed a different dipping behavior between internal multiples and signal in the $x - h_x$ space underneath the salt. In general, the power of stacking can attenuate certain migration artifacts if they are not consistent across the images.

We propose using a different approach to remove unwanted noise in migration images based on assumptions about a range of possible dips in the ADCIG. In addition to multiples, this method can address many types of migration artifacts. The physical meaning of the filter is very intuitive. Users need to determine an angular range for signal to form in each subsurface location for each prestack shot gather. Such an angular range can be determined with illumination analysis. This noise filtering scheme is particularly suitable for gradient conditioning in least-squares reverse-time migration (LSRTM).

We will first explain the theory behind shot-image gather angle-domain noise filtering in 2D. Next, we will show the performance of the filter on an RTM image with a field dataset. Finally, we will compare the results of LSRTM with and without noise filtering. We found that LSRTM with noise-filtering converges to a more realistic solution, especially in area where unwanted noise is the most prominent.

THEORY

The assumption behind shot-gather angle-domain filtering is that noise and signal are formed at different angles for each shot gather. While this assumption is not true for all kinds of noise, it is useful as a way to alienate certain types of noise in the images. In this report, we use an ocean-bottom node (OBN) field dataset from the Deimos field (Wong et al., 2013) as an example. In OBN survey, reciprocity is applied in which the role of shots and receivers are exchanged. Prestack migration images are calculated by receiver gathers. For simplicity, we will refer to an OBN image gather as a shot gather. Figure 1a shows a shot image gather generated by a single ocean-bottom node (OBN) at $x_{\text{OBN}} = 54150$ m and $y_{\text{OBN}} = 34800$ m. Figure 1b,c, and d are displaying the depth-angle panel of Figure 1a at 3 different inline locations of 53000 m, 54000 m, and 55000 m. These depth-angle panels are located to the left, around, and to the right of the ocean bottom receiver along the inline direction. There are several characteristics based on the image gather. Image points near the receiver are mostly illuminated by reflections with small aperture angles. On the other hand, image points located to the left of the receiver are predominantly illuminated by reflections with negative aperture angles as shown in Figure 1b. The opposite result is true for Figure 1d with the image point located to the right of the receiver. Similarly, image points located to the right of the receiver are predominantly illuminated by reflections with positive aperture angles as shown in Figure 1d.

We can identify areas of signal and noise in Figure 1 by slicing through the angle domain. Figure 2a shows the image extracted at an subsurface angle of 15 degrees. At this illumination angle, the image is predominantly signal (label 1). Figure 2c is

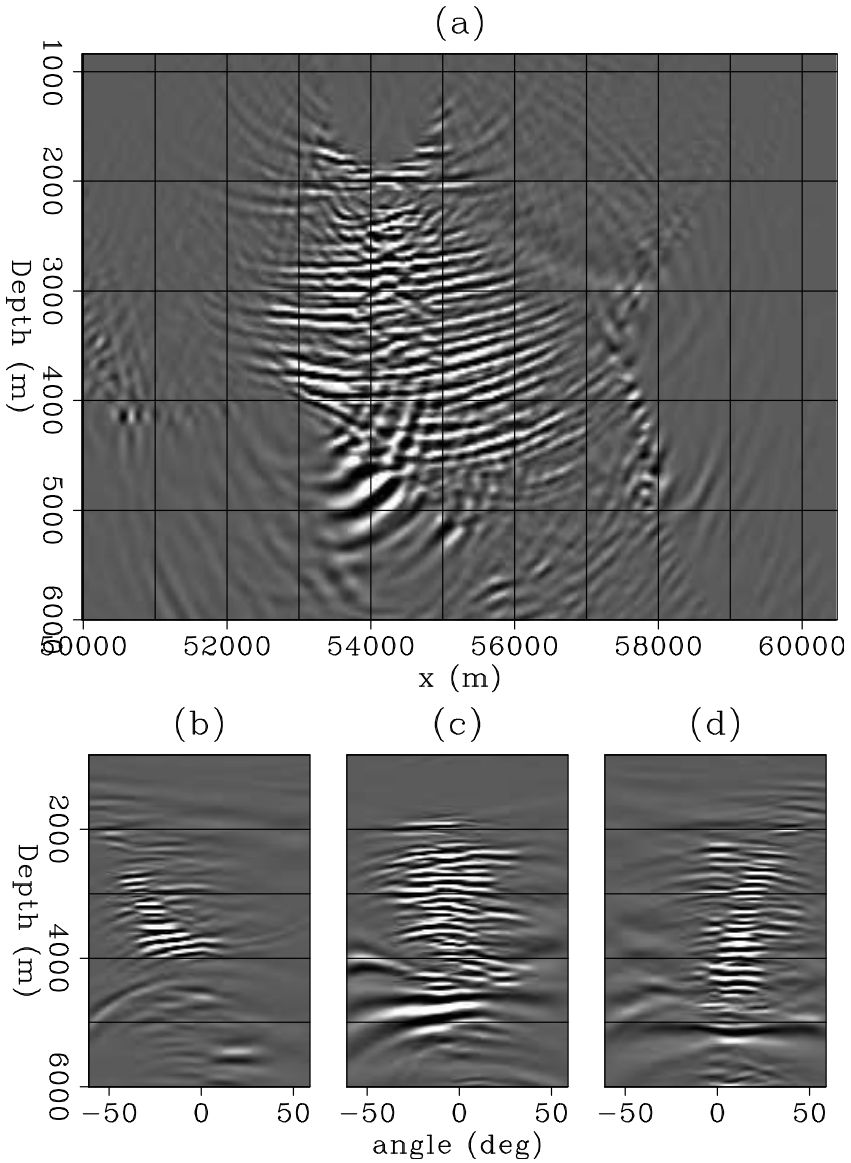

Figure 1: An 2D RTM image generated with an ocean-bottom receiver located at $x_{\text{OBN}} = 54150m$ and $y = 34800m$. Depth-angle panels are taken at inline locations of (b) x=53000 m, (c) 54000 m, and (d) 55000 m. The prominent energy in the depth-angle panel is shifted based on its relative position from the source. [**CR**]

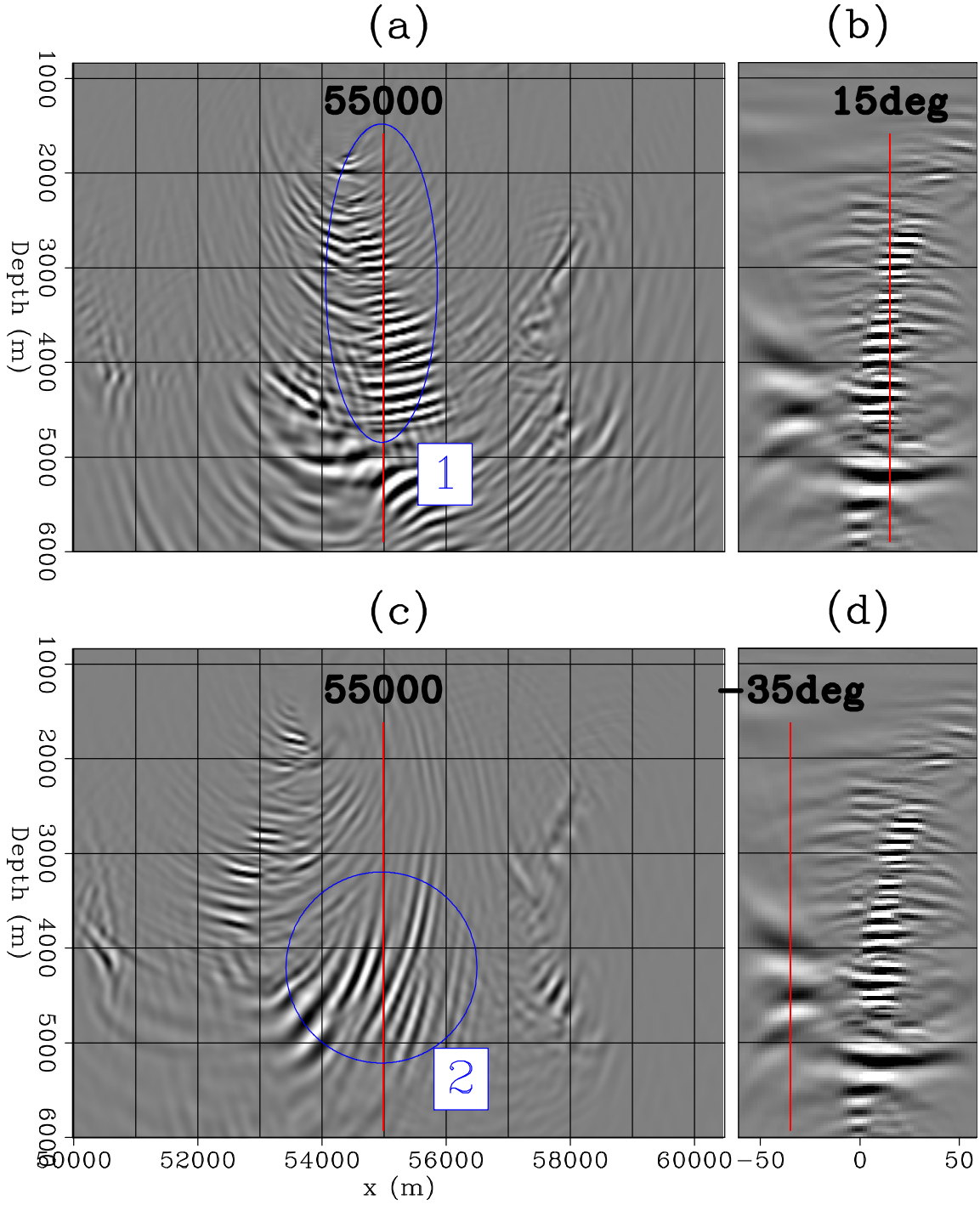

Figure 2: The same image gather from Figure 1. (a) is showing the image illuminated at an angle of 15 degrees. Label 1 highlights an area that is predominantly signal. (b) is showing the corresponding depth-angle panel extracted at midpoint x=55000m with a line indicating the slicing of the image cube at 15 degrees. (c) is showing the image illuminated at an angle of -35 degrees. Label 2 highlights an area that has conflicting dips with the sediment and is believed to be noise. (d) The same depth-angle panel as in (b) but with a line indicating the -35 degrees slicing. [**CR**]

showing an area (label 2) that is believed to be migration artifacts and is illuminated at -35 degrees.

It is important to highlight the benefit of filtering at each prestack-shot image gather instead of at a poststack image gather. This extra degree of freedom allows us to isolate noise that would have otherwise be stacked with the signal in a poststack image gather. However, as mentioned before, the power of stacking in itself can eliminate some of those noises while leaving noise that are consistent across all the shot gathers. A good test is to compare the result of noise filtering between applying to each prestack ADCIG and applying to a single poststack ADCIG. We have yet to make this comparison.

Given that we have identified an angular range to be signal for each shot-image gather, it is straight-forward to remove the noise. In two dimension, filtering in the angle domain is equivalent to filtering the dips in the depth-offset domain. The relationship between the dips in the depth-offset domain to the aperture angle (γ) is,

$$\frac{k_{\text{hx}}}{k_z} = -\tan\gamma. \tag{1}$$

where k_{hx} and k_z are wavenumber along the subsurface offset (hx) and depth z directions. In practice, we apply the filter in the depth-offset domain by finding equivalent dips ranges based on the angle ranges using equation 1. Although equation 1 is only true in 2D, there is an equivalent expression in 3D that includes the reflector's tilt. For this particular dataset, there is not enough crossline aperture to obtain a meaningful extended image gather in the crossline direction. An equivalent filtering procedure involving k_{hy} can be applied in 3D.

EXAMPLE

A single shot-gather

Figure 3a shows the result of extended domain filtering on a prestack OBN image. Most of the noise is removed above the salt reflection at $z = 4000m$. Figure 3b, c, and d, are displaying the depth-angle panel of Figure 3a at x=53000 m, 54000 m, and 55000 m. The angle range are chosen to preserve the prominent energy in the image. Figure 4a shows the corresponding filtered noise. Figure 4b, c, and d, are displaying the depth-angle panel of Figure 4a at x=53000 m, 54000 m, and 55000 m. The original prestack RTM image (Figure 1a) is decomposed into the signal part (Figure 3a) and the noise part (Figure 4a).

Least-squares RTM

In addition to removing noise in RTM, the same noise-filtering method can also be used in least-squares RTM (Wong et al., 2010). We use conjugate direction to

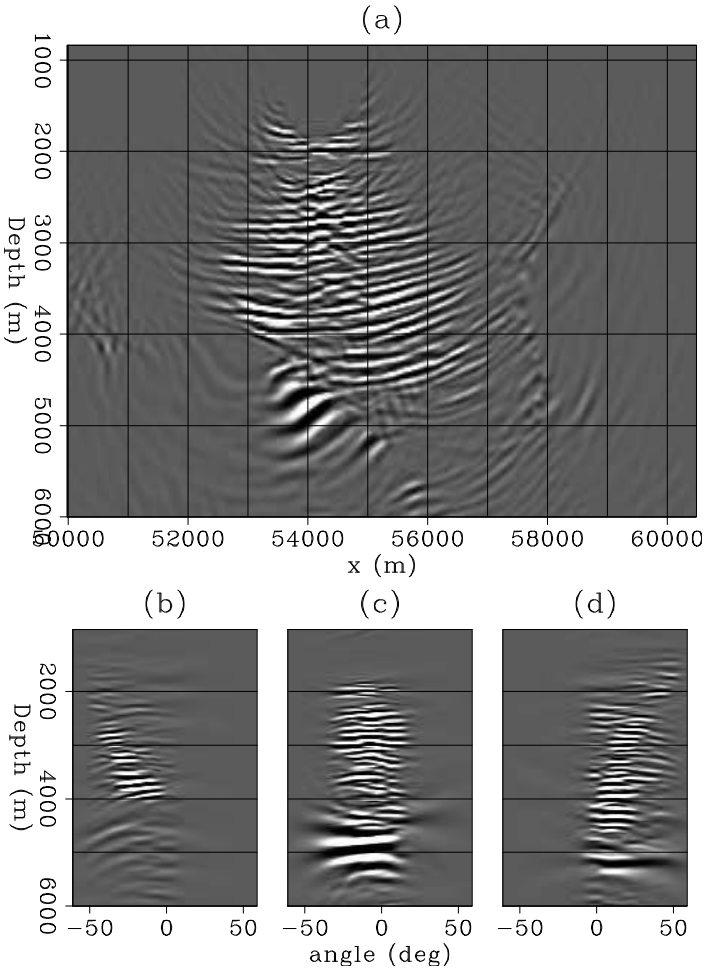

Figure 3: The same prestack RTM image as in Figure 1 after extended-angle domain filtering. Depth-angle panels are taken at inline location of (b) x=53000 m, (c) 54000 m, and (d) 55000 m. [**CR**]

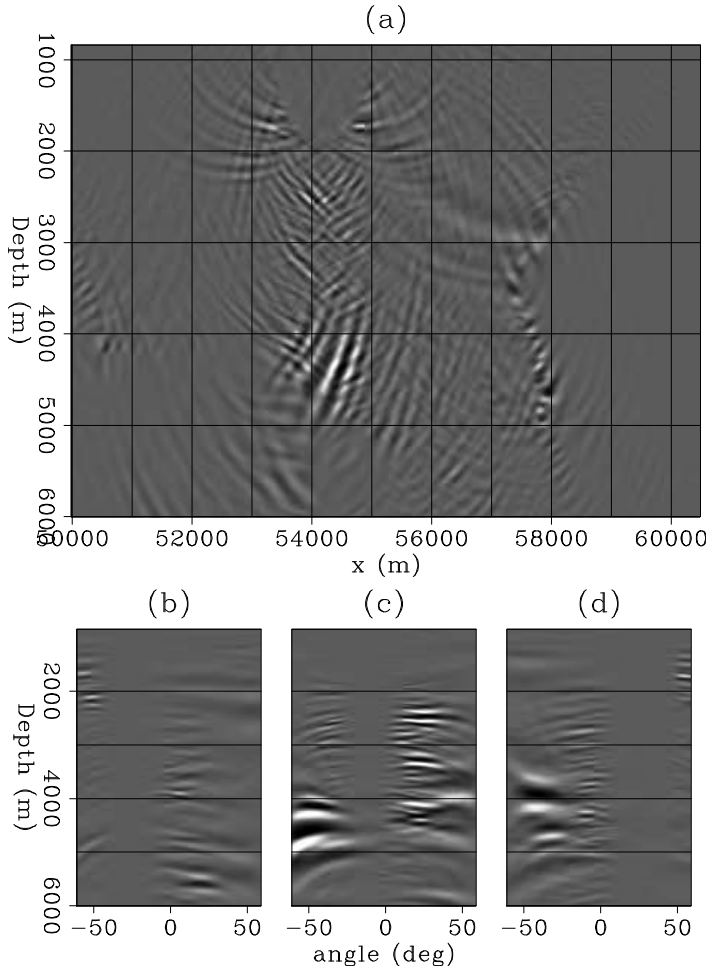

Figure 4: The filtered noise from the same prestack RTM image as in Figure 1 after extended-angle domain filtering. Depth-angle panels are taken at inline location of (b) x=53000 m, (c) 54000 m, and (d) 55000 m. The sum of Figure 3a and Figure 4a should be the same as Figure 1a [**CR**]

perform iterative inversion in LSRTM. At each iteration step, we apply the same filtering onto the gradient. Figure 5 shows the stacked RTM image with filtering, the stacked RTM image without filtering, and the differences (or the filtered noise). All three images in Figure 5 are displayed with the same clip. There are several areas in Figure 5 that has conflicting dips. Label 1 and 2 highlight regions where the noise is the most prominent. After 20 iterations of LSRTM, the inverted images are shown in Figure 6. When compared with the RTM image, the LSRTM image has higher resolution and better relative amplitude information. However, there is also more noise in the LSRTM image. This is the result of the various scattering in off the sharp velocity contrast in the background velocity model. A simple synthetic LSRTM test with and without a sharp background velocity will highlight this issue. These noise are often incoherent and tends to fall into the null space of the inversion problem. The LSRTM-image with noise-filtering (Figure 6b) has an overall cleaner result. In addition, a region where sediments truncate against a salt flank (label 3) appears to be better imaged when noise-filtering is applied.

DISCUSSION

How to choose the angle range?

Because our field data example is relatively small, the angle-range used in the filtering is hand-picked by observing a few shot-image gather. However, for large datasets, the angle-picking can be automated by illumination analysis. Gherasim et al. (2014) apply angle based illumination weighting onto their poststack image. Instead of applying the analysis onto the poststack image, the same analysis can be applied to the prestack shot-gather image.

What if true signal in the image is filtered out?

One potential danger of this method is unintentionally filtering out true signals in the image. This can happen when the angle-range chosen is too restrictive. One way to help alleviate this problem is to identify challenging subsurface regions where we want to avoid any filtering. For example, areas against a salt flank or subsalt would be considered challenging.

What is the computational cost of applying this filter?

This filtering method requires subsurface-offset gather to be computed, which drastically increase the computational cost of conventional LSRTM. Therefore, it is more suitable for LSRTM or LSM which is already calculating the extended gather for amplitude-verse-angle (AVA) analysis (Kuehl and Sacchi, 2003). The filtering itself involve 2D Fourier transforms of the image cube at the end of each migration. In 2D,

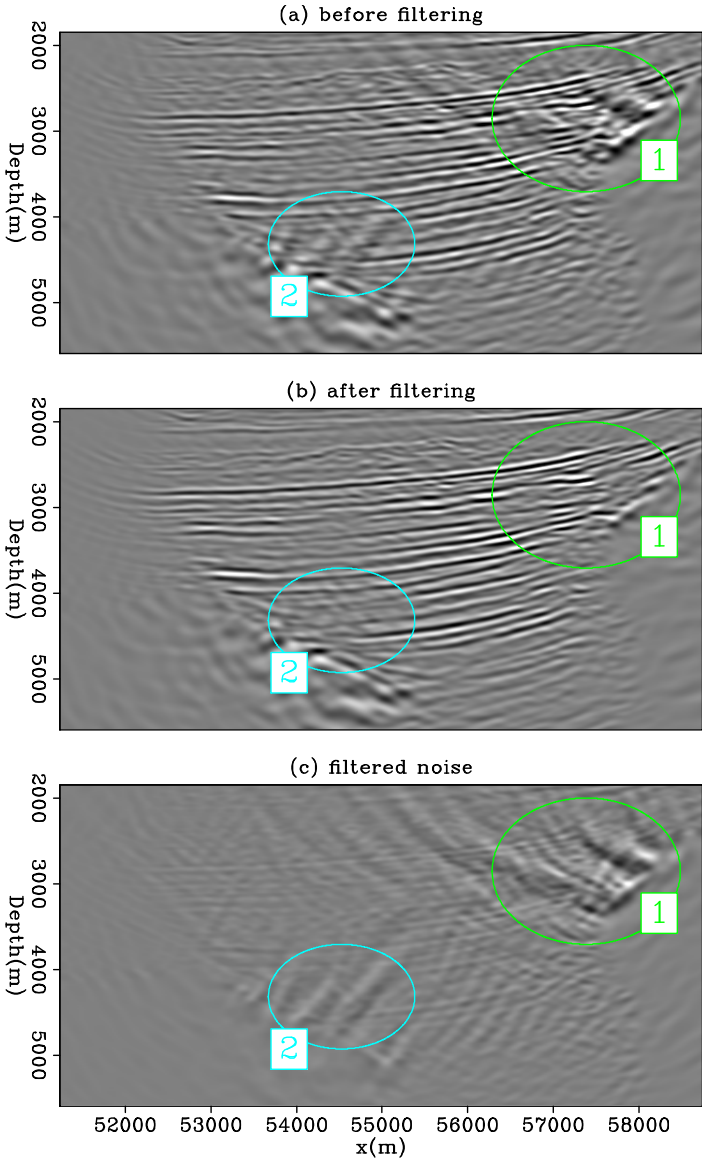

Figure 5: (a) RTM without filtering, (b) RTM with filtering, and (c) the differences between (a) and (b). All images are displayed at the same clip. Label 1 and 2 highlight regions where the noise is the most prominent.

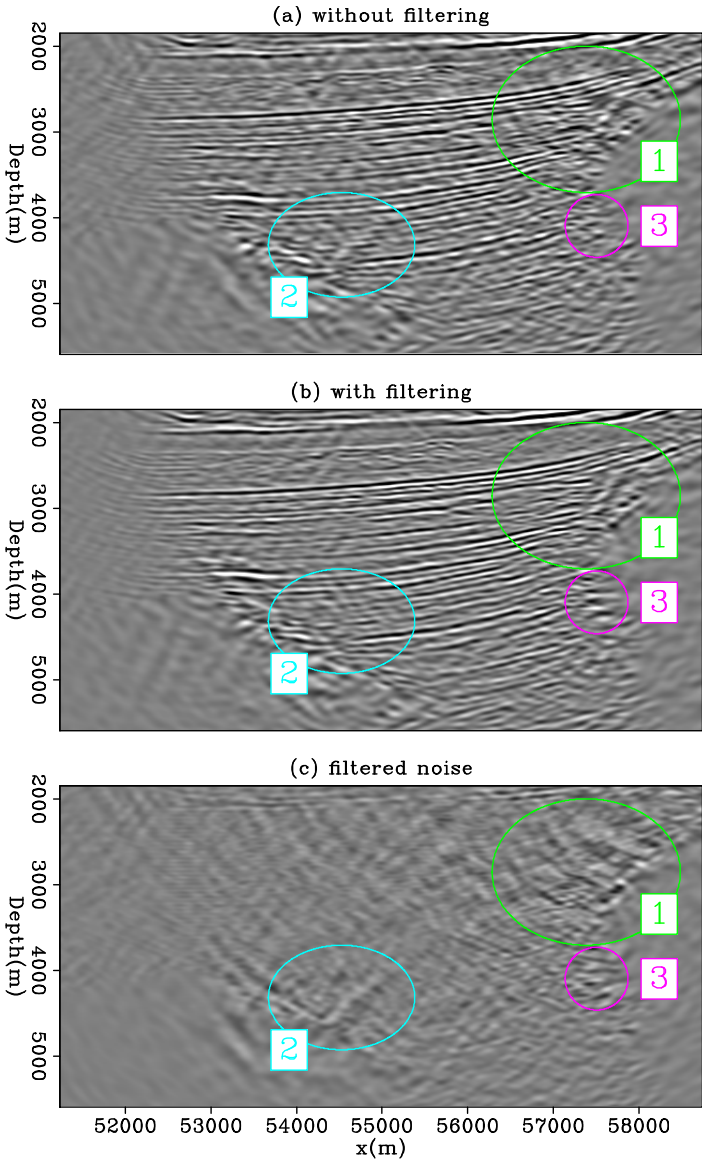

Figure 6: (a) LSRTM without filtering, (b) LSRTM with filtering, and (c) the differences between (a) and (b). All images are displayed at the same clips. Label 1 and 2 highlight regions where the noise is the most prominent. Label 3 point to a region where the sediment against a salt flank is better imaged in (b) than in (a).

the computational cost of each shot-domain angle gather is $\propto n_x n_z n_h n_t$ where n_x, n_z, and n_h are the size of our image cube in the x, z, and offset directions. n_t is the number of time steps in the time-domain finite-different calculation. The cost of noise filtering onto each ADCIG is $\propto n_x n_z n_h log(n_z n_h)$. In most application, the value of $log(n_z n_h)$ is much less than n_t. The cost of filtering is relatively less expensive than the computational cost of migration.

CONCLUSION

We present a method to remove unwanted noise in reverse-time migration by discriminating in the prestack shot-gather angle domain. This method involves identifying angular ranges that are attributed to signal in the subsurface for each prestack image gather. Our field data example shows that some migration artifacts or noise can be removed from the RTM image. We also find that shot-gather angle-domain noise filtering helps improve least-squares reverse-time migration result.

ACKNOWLEDGMENTS

The author wish to thank Shell Exploration and Production Company, as well as BP Americas for permission to publish this work. We also thank Michael Merritt, Richard Cook, Colin Perkins, Vanessa Goh, and Alexander Stopin for their data processing, helpful suggestions and discussions.

REFERENCES

Alvarez, G., B. Biondi, and A. Guitton, 2007, Attenuation of specular and diffracted 2D multiples in image space: Geophysics, V97–V109.

Gherasim, M., B. Nolte, J. Etgen, P. Jilek, P. Vu, M. Trout, and K. Hartman, 2014, Wave-equation angle-based illumination weighting for optimized subsalt images: The Leading Edge, **33**, 392–399.

Kuehl, H. and M. D. Sacchi, 2003, Least-squares wave-equation migration for AVP/AVA inversion: Geophysics, **68**, 262–273.

Riley, D. C. and J. F. Claerbout, 1976, 2D multiple reflections: Geophysics, **41**, 592–620.

Tsai, C. J., 1985, Use of autoconvolution to suppress first-order long period multiples: Geophysics, **50**, 1410–1425.

Valenciano, A. A., 2008, Imaging by wave-equation inversion: PhD thesis, Stanford University.

Verschuur, D. J., A. J. Berkhout, and C. P. A. Wapenaar, 1992, Adaptive surface-related multiple elimination: Geophysics, **57**, 1166–1177.

Wong, M., B. Biondi, and S. Ronen, 2010, Joint least-squares inversion of up- and down-going signal for ocean bottom data sets: SEG Expanded Abstracts, 2752–2756.

———, 2013, Joint-lsrtm in practice with the deimos ocean bottom field dataset: Stanford Exploration Project Report, **150**.

Yilmaz, Ö., 1991, Seismic data processing. Investigations in geophysics: Soc. of Exploration Geophysicists.